ARTICLES

Individual and Collective Electronic Properties of Ag Nanocrystals

S.-H. Kim,*,† G. Medeiros-Ribeiro,‡,§ D. A. A. Ohlberg,‡ R. Stanley Williams,‡ and J. R. Heath†

Hewlett-Packard Labs, 3500 Deer Creek Road, MS 26U-12, Palo Alto, California 94304-1392, and Department of Chemistry and Biochemistry, UCLA, Los Angeles, California 90095-1569

Received: June 14, 1999

We report on the electronic transport properties of individual alkanethiol-passivated Ag nanocrystals and their superlattices. Isolated Ag particles with diameters in the range of 2.7−4.8 nm supported by a metallic substrate passivated with an organic layer show a Coulomb gap. Monolayer films of Ag particles exhibit four distinct electronic signatures, two of which have not been previously reported, depending on their structures. In two-dimensional ordered superlattices of octanethiol-capped 4.8 nm diameter nanocrystals on graphite, the strong interparticle electronic coupling produces metallic films. A disordered monolayer of dodecanethiol-capped 6.6 nm diameter nanocrystals exhibits a temperature-dependent differential conductance, which is attributed to the localized states formed by the disorder in the lattice. For two-dimensional ordered superlattices of pentanethiol- and hexanethiol-capped 2.7 nm diameter Ag particles, we find that the films are insulating, and individual nanocrystals maintain their individual electronic identity. Two different types of insulating films have been observed: one with electronically homogeneous nanocrystals in a close-packed lattice and the other with sublattices of electronically distinct nanocrystals within a square lattice. We discuss the relationship of the Coulomb blockade and nanocrystal ordering to the electronic behavior of this class of architectonic materials.

1. Introduction

The ability to design the macroscopic electronic and optical properties of a solid by so-called "band-gap engineering" has produced many important devices as well as advances in the basic understanding of carrier confinement in solids. Yet, control in two and three dimensions, with the same precision that one has along the growth direction with heteroepitaxial techniques, has not been accomplished. There are, however, attempts along these lines in strained heteroepitaxial systems. The degree of ordering is slowly improving[1] despite the fact that the nanostructures themselves suffer from finite size dispersions.[2]

An alternative approach toward electronic-structure engineering in two and three dimensions is to utilize chemically synthesized and assembled nanocrystals (NCs) as the building blocks for a solid. High-quality NCs of both metallic and semiconducting systems are now readily available, and the preparation of two- and three-dimensional superlattices of those NCs is now well established.[3,4] One major difference that distinguishes NC superlattices from those grown using thin-film techniques is that a chemically prepared NC typically consists of an inorganic core (the actual nanocrystal) capped with an organic surfactant. This means that, at the very minimum, each NC in the superlattice is separated from every other by an insulating (tunneling) barrier. Nevertheless, if metal NC superlattices can be prepared so that the separation distance between the cores of adjacent NCs is sufficiently small, then strong quantum mechanical exchange coupling can be observed.[5,6] The ability to tune such exchange coupling correlates directly with the ability to custom design the electronic properties of an "architectonic" solid using a NC, or "artificial atom", as a basis. Recent experiments on Langmuir monolayers of Ag NCs have demonstrated that a reversible Mott-type metal−insulator (MI) transition could be "designed" into a NC superlattice.[7] In a superlattice of weakly interacting silver NCs, the electronic structure of the superlattice is that of an insulator with a Coulomb gap, which arises from the charging energy of the NC lattice sites. As the lattice is compressed, exchange coupling between NC lattice sites leads to a decrease in kinetic energy of the isolated NC wave functions, which, in turn, reduces the Coulomb gap. At the insulator-to-metal transition, the Coulomb gap disappears and the superlattice can become a metallic film. We previously observed the disappearance of this gap by using temperature-dependent scanning tunneling microscope (STM) measurements on two-dimensional superlattices that were prepared on either side of the MI transition.[8] In this paper, we again use temperature-dependent STM measurements to probe more deeply into the electronic properties of Ag NC superlattices at various levels of exchange coupling—from completely isolated particles to a superlattice that exhibits true metallic character. Our goal is to explore the phenomenology and the physics associated with electronic structure rehybridization in these systems, to begin addressing the role of disorder

* Corresponding author. Current address: Hewlett-Packard Labs, 3500 Deer Creek Road, MS 26U-12, Palo Alto, CA 94304-1392. E-mail: sangho@hpl.hp.com.

† UCLA.

‡ Hewlett-Packard Labs.

§ Present address: Laboratório Nacional de Luz Síncrotron, PO Box 6192, Campinas, SP 13083-970 Brazil.

10.1021/jp991952y CCC: $18.00
Published on Web 11/04/1999

in NC superlattices, and eventually to understand how to intentionally design systems with desired electronic properties.

2. Experimental Details

The preparation of Ag NCs has been previously described.[9,10] Once the particles were prepared, the dodecanethiol surface groups could be readily exchanged to produce NCs that were passivated with pentanethiol, hexanethiol, or octanethiol. For the shortest surface groups, the NCs coarsened after just a few hours at room temperature, and so experiments on those NCs were carried out immediately after preparation. The particle sizes were determined using UV/vis absorption spectra that had been correlated with transmission electron microscope (TEM) measurements of particle size. Particle sizes measured in this way were in good agreement with the STM measurements.

For experiments on isolated NCs, commercially available (111) oriented Au on mica substrates were immersed into a 1 vol % hexanedithiol in acetone solution to make a dithiol monolayer. These substrates were then immersed into a very dilute Ag particle solution (<0.1 mg/mL) for 5−10 s. In this way, a low coverage of Ag NCs on the substrate could be prepared. The particles were further fixed to the substrate by dipping the wafer into the dithiol/acetone solution, and then rinsing the wafer in hexane to remove any unattached particles.

For the NC monolayer experiments, Langmuir films of Ag NCs were transferred to highly oriented pyrolytic graphite (HOPG) substrates at various surface pressures prior to monolayer collapse.[9] It was difficult to prepare uniform monolayers of the larger NCs because the strong interparticle dispersion interaction between those particles caused the NCs to aggregate into islands.[11] In order to make uniform films, we therefore allowed the Langmuir monolayer to relax for as long as 2 h, and the relaxation was monitored by surface pressure measurements. This procedure was found to effectively anneal smaller two-dimensional islands of NCs into a continuous monolayer, thereby improving the crystallinity of the NC monolayer.

The imaging and transport experiments were performed in a ultra-high-vacuum (UHV) STM at low temperatures. The positional stability of the NCs depended on the length of the thiol chains, with longer chains allowing more movement and poorer signal/noise ratio in the current−voltage ($I-V$) measurements. All STM experiments were initiated within 3 h of film preparation. All experiments were repeated several times with different particle batches, and the results presented in this work were representative of and consistent with the more comprehensive data set.

3. Experimental Results

3.1. Coulomb Blockade on Isolated Particles. Tunneling spectroscopy on single metal NCs has been previously reported.[12] The substrate can, in principle, have a very strong influence on the spectroscopy of the NC superlattices—especially for the case of an Au substrate. In order to evaluate this influence, we measured the voltage-dependent tunneling current through isolated metal NCs that were chemically attached to an atomically flat Au substrate using hexanedithiol linking molecules. Figure 1 summarizes the results for 2.7 nm particles.

The upper portion of Figure 1a represents a current image (collected at constant tip height) at voltages lower than the Coulomb gap in current imaging tunneling spectroscopy (CITS) experiments. Brighter areas correspond to high current flow and dark areas correspond to little or no current flow. Thus, this is a map of the Coulomb gap at the surface. A topography image, which was simultaneously acquired, is shown at the bottom of Figure 1a. The electronic character of the particles is clearly insulating at the imaging bias ($V_{sample} = 0.22$ V), indicating a density of states different than that of the metallic substrate. Tip geometry artifacts can be ruled out, as one would expect an increase in current (rather than the observed decrease) due to a topographic induced lowering of the barrier height at the edges of the particle.[13] Figure 1b exhibits the differential conductance (dI/dV) characteristics of the bare substrate and on two Ag NCs. One can see the Coulomb gap as well as the first few Coulomb charging steps of the NCs.

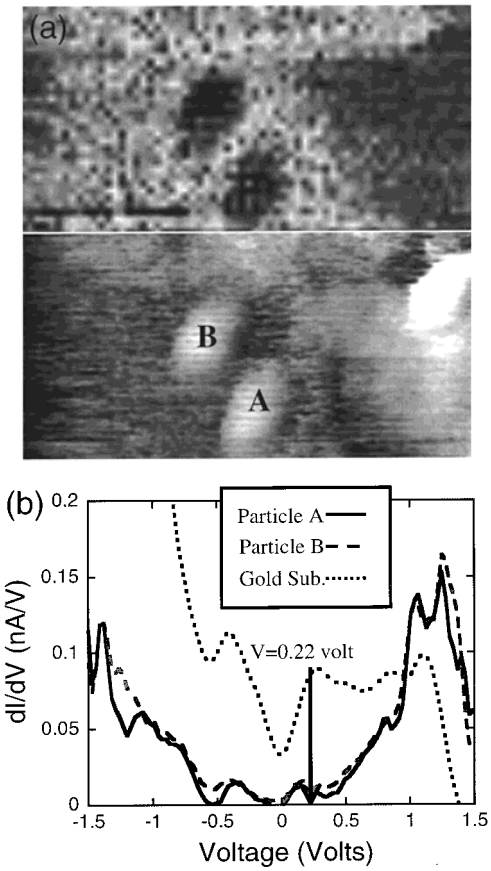

Figure 1. (a) 25 nm × 12.5 nm CITS (upper image, at 0.22 V) and STM (lower image) scans on 2.7 nm diameter isolated Ag particles. In the CITS image (see text for details), white corresponds to more current and black to little or no current, indicating a blockade behavior for the particles. The nanoparticles appear elongated because of instrumental drift during the slow scan required to collect spectroscopic I−V data. (b) dI/dV spectra collected from the Ag nanocrystals in (a) (marked "A" and "B") and on the hexanedithiol-coated Au(111):mica substrate. Note the metallic character of the substrate and the Coulomb gap and staircase of the Ag nanocrystals. The arrow indicates the voltage at which the CITS image in (a) was collected.

Similar experiments were performed on a different NCs of varying sizes and ligand lengths. A distinct Coulomb gap and accompanying blockade behavior was always observed.

3.2. Nanocrystal Monolayers. We examined a variety of NC monolayers. For different NC diameters, we prepared films in which the NC separation was varied by changing the ligand length and the pressure applied to the film. Table 1 summarizes the parameter space explored in previous[8] and the present work. Because of various experimental limitations, it was not possible to prepare monolayer films with arbitrary combinations of NC size and ligand.

TABLE 1: Samples Studied in the Present and Previous Work[7]

		particle size (nm)			
		2.7	4.8	6.6	7.2
ligand type	C_5/C_6	M,[8] I[b]			
	C_8		M		M
	C_{12}	I[8]		*Inter*	

[a] I represents superlattices in the insulating state, M represents superlattices in the metallic state, and *Inter* represents sample in an intermediate state. [b] This insulating superlattice was prepared at low surface pressure on the Langmuir trough.

3.2.1. Metallic Monolayers. We investigated monolayer films of 4.8 nm octanethiol-passivated particles with an estimated $D/2r$ ratio of 1.25, where D is the particle center-to-particle center separation distance and r the radius of the Ag core. Figure 2, a and b, shows 250 nm × 250 nm and 50 nm × 50 nm STM images, respectively, of these films. The wide scan shows a long-range buckling of the film, which at its maximum is measured to be just less than a single particle high, implying the film does not have multilayer islands. This was independently confirmed during the film preparation, as no monolayer collapse was detected either optically or from the pressure/area isotherm measurements. This long-range buckling is apparently due to the strong particle−particle attractions that characterize large particles. Although this film is not in uniform contact with the underlying substrate, the observed electronic properties are invariant with respect to location over the entire film. This can be seen in Figure 2c where we present two dI/dV curves, collected at the high and low regions of the buckled film. The conductance at 0 V for this film is finite valued and temperature independent, which indicates that this film is truly and homogeneously metallic.

3.2.2. Hopping-Conductivity Monolayers. Monolayer films of 6.6 nm dodecanethiol capped Ag NCs were prepared on HOPG substrates, and Figure 3a is an STM image, which shows that these were relatively disordered films. We estimate that $D/2r$ for this film is about ∼1.3, which is close to what has been previously observed to produce a metallic film.[7] The temperature-dependent differential conductance spectra are presented in Figure 3b. These plots are smooth, with no evidence of a Coulomb gap. However, at zero bias the conductance clearly increases with temperature, demonstrating that the film is not metallic. In order to determine the nature of the electron transport in these films, we fit the zero-bias conductances at several temperatures using various thermally activated hopping models. [14] Variable-range hopping (VRH) theory[15] yields the best fit to our data, as shown in the inset in Figure 3b. From the VRH theory, the dependence of conductivity (σ) on temperature (T) is

$$\sigma(T) = \sigma_0 \exp[-(T_0/T)^{\phi}] \qquad (1)$$

where $T_0 = \beta/k_B g(\mu) a^d$ $g(\mu)$ is the density of states (DOS) at the Fermi level, a is the localization radius of states near the Fermi level, d is 2 for two-dimensional and 3 for three-dimensional systems, and β a numerical constant (∼13.8 and ∼21.2 for for two- and three-dimensional systems, respectively). The exponent ϕ is related to the dimensionality of the system, $\phi = 1/3$ for two and $\phi = 1/4$ for three dimensions. Fits to both values of ϕ yield essentially the same standard deviation. However, for $\phi = 1/4$, we obtain a localization radius (a) of ∼1.2 nm, while for $\phi = 1/3$, $a \sim 2.8$ nm. This second value is more physically reasonable (the radius of single a Ag particle is 3.3 nm), especially considering that the film is a single monolayer.

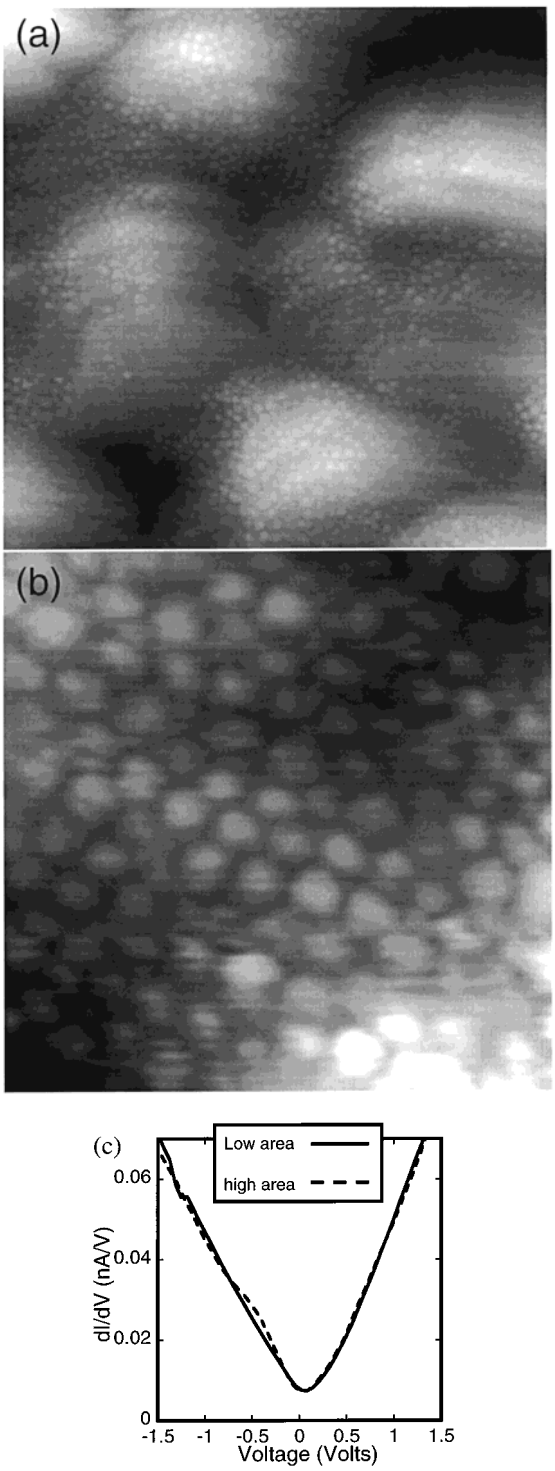

Figure 2. (a) 250 nm × 250 nm and (b) 50 nm × 50 nm STM scans on a monolayer of octanethiol-passivated 4.8 nm diameter Ag nanocrystals. Note the buckling in (a) (see text), which is about 5 nm between the lowest and highest points. (c) dI/dV spectra collected at low (solid line) and at high (dashed line) areas on the film. Note the metallic character for both curves, demonstrated by the finite conductance at zero bias.

3.2.3. Insulating Monolayers. (a) Hexagonal Lattice: Electronically Homogeneous. Monolayer films of 2.7 nm hexanethiol-capped Ag particles were transferred to HOPG substrates and imaged at 20 K in a UHV-STM chamber. We estimate that $D/2r$ for this film to be around ∼1.4. In Figure 4a, we present a 50 nm × 50 nm STM image of a network of insulating particles on HOPG. The image shows a reasonably

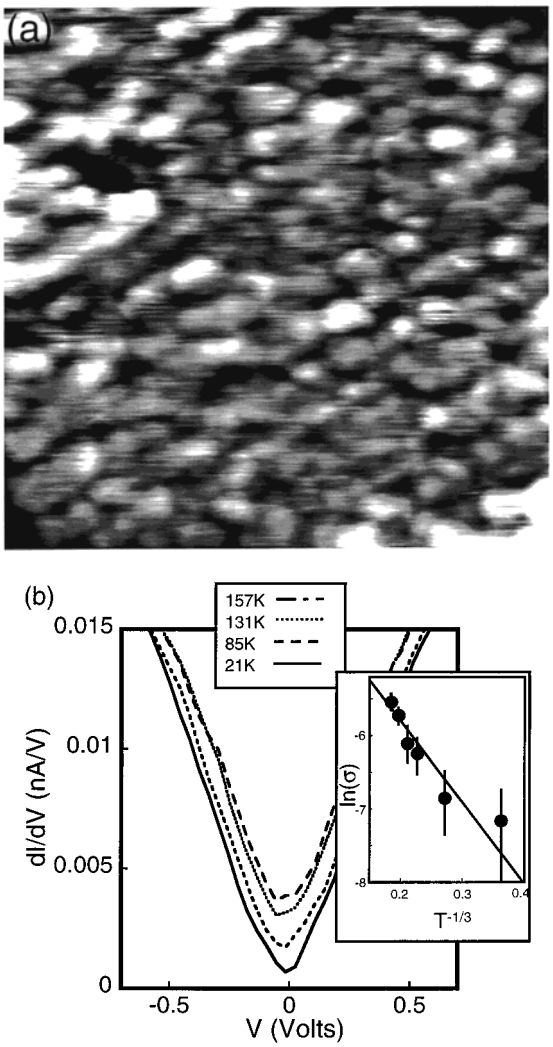

Figure 3. (a) 100 nm × 100 nm STM scan on a monolayer of dodecanethiol passivated 6.6 nm diameter Ag nanocrystals. The image looks blurred because of the long ligands on the surface. (b) Temperature-dependent differential conductance plot for a hopping conductivity monolayer. The conductivity at the Fermi energy is explained well by the variable range hopping (VRH) model for a two-dimensional system (inset). Each circle (●) represents an experimental datum and the solid line is the fitted line.

well-ordered hexagonal lattice with a low density of vacancies. Differential conductance measurements shows that all the NCs exhibit similar electronic structures. The normalized differential conductance (NDC), d*I*/d*V* ·*V*/*I*, which is an approximate measurement of the DOS for this film is plotted in Figure 4c. The Coulomb gap from this plot is ∼200 meV (fwhm), in good agreement with the calculated charging energy.

(a) Square Lattice: Electronically Heterogeneous. Figure 4b shows another 50 nm × 50 nm STM image of a monolayer of 2.7 nm pentanethiol-capped Ag NCs. This film was prepared at lower compression (surface pressure, $\pi = 5$ mN/m) than the hexagonal film ($\pi = 8$ mN/m) and exhibits a square-lattice structure with moderate disorder. Because of the relatively large particle separation distances, the difference in tunneling current at and between the NCs can be observed. The top panel in Figure 5a corresponds to a 25 nm × 12.5 nm current image collected at a voltage (0.22 V). The 2.7 nm Ag particles block nearly all the current at that bias, whereas the HOPG substrate has a high conductance. The bottom image is the simultaneously collected topographic map of the same 25 nm × 12.5 nm area.

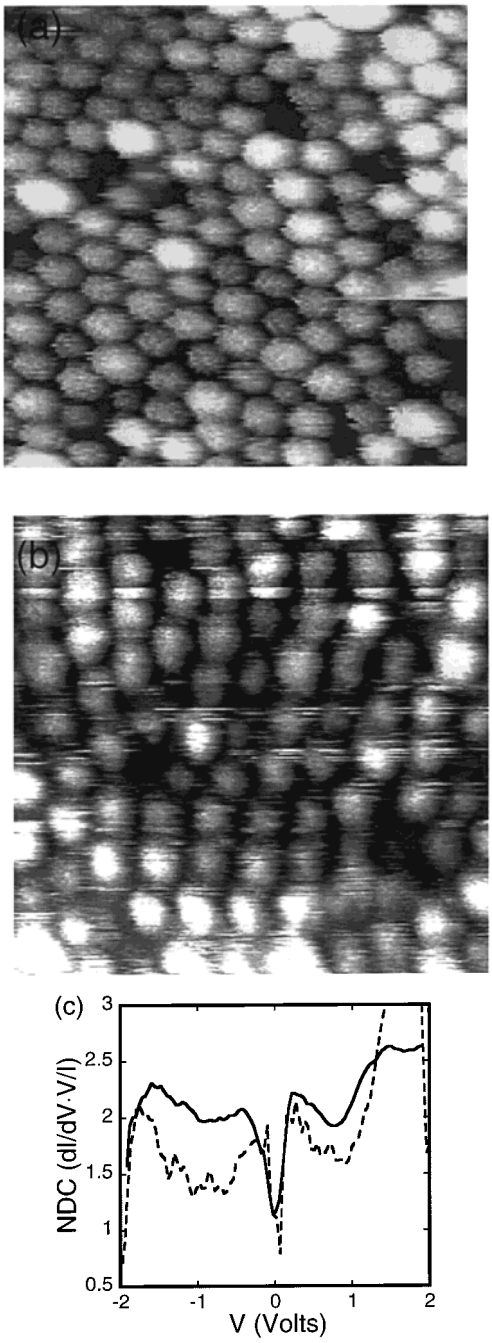

Figure 4. 50 nm × 50 nm STM scans of electronically (a) homogeneous (film A) and (b) heterogeneous (film B) films. Film A consists of 2.7 nm diameter particles with hexanethiol ligand and prepared at $\pi = 8$ mN/m. Film B consists of 2.7 nm diameter particles with pentanethiol ligand and prepared at $\pi = 5$mN/m. (c) NDC (d*I*/d*V*·*V*/*I*) for film A (dashed line) and film B (solid line). The wide gap particles are excluded in calculating NDC for film B. Note the plots are smoothed with 0.2 eV window causing nonzero NDC at $V = 0$ V. All the measurements were carried out at 20 K.

We also examined the differential conductances of the individual NCs in this superlattice. We observed two electronically distinct NCs: type "W" particles with a wide gap (∼0.8 V) and type "N" particles with a narrower gap (∼0.25 V), as shown in Figure 5b. The two electronically different NCs are distributed on nearly-equally populated but disordered sublattices, as indicated by the "N" and "W" labels in the bottom panel of Figure 5b.

The unusually wide Coulomb gaps of type "W" NCs motivate us to carefully scrutinize the results for this type of insulating

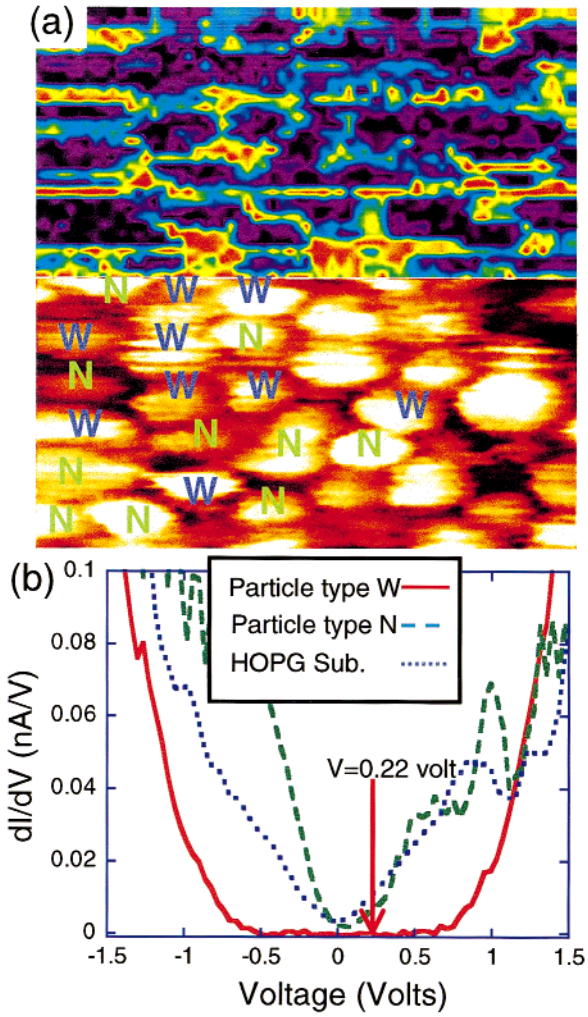

Figure 5. (a) 25 nm × 12.5 nm CITS (upper image) and STM (lower image) scans on a monolayer of pentanethiol passivated Ag nanocrystals (2.7 nm diameter) in the insulating state (film B in Figure 4). In the CITS image (see text for details), bright yellow corresponds to more current and dark purple to little or no current, indicating a blockade behavior in each nanoparticle. The color scheme is the same as in Figure 6b. (b) d*I*/d*V* spectra collected from different areas in (a). Spectra for type "W" and type "N" particles are solid and dashed lines, respectively. The substrate (HOPG) spectrum was collected between particles and reveals a nonzero conductance at zero bias voltage, as expected for a semi-metal at finite temperature. The arrow indicates the voltage where the CITS image in (a) was taken.

film. In Figure 6a, an STM topographic map of three Ag NCs is presented. Figure 6b shows the corresponding current image as a function of topographic direction along the axis of the NCs and bias voltage along the perpendicular axis. The Coulomb gap of the middle particle appears to decrease from right to left, suggesting that particles may influence the electronic states of their neighbors.

4. Discussion

In our experiments on Ag NC monolayers, we have identified four electrically discrete types of film. Metallic and homogeneous insulating films have been discussed previously.[8] Here, we discuss the two new behaviors and examine the issues that affect them all.

4.1. Localized Insulator. A crucial parameter in the NC superlattices is obviously the particle size and interparticle separation distance. We have studied the effects of various combinations of size and separation throughout this paper. In addition to the effects from these two parameters, the effect of disorder in this system has been studied in section 3.2.2. We have observed the temperature-dependent differential conductance change and have applied VRH theory to explain this phenomenon.

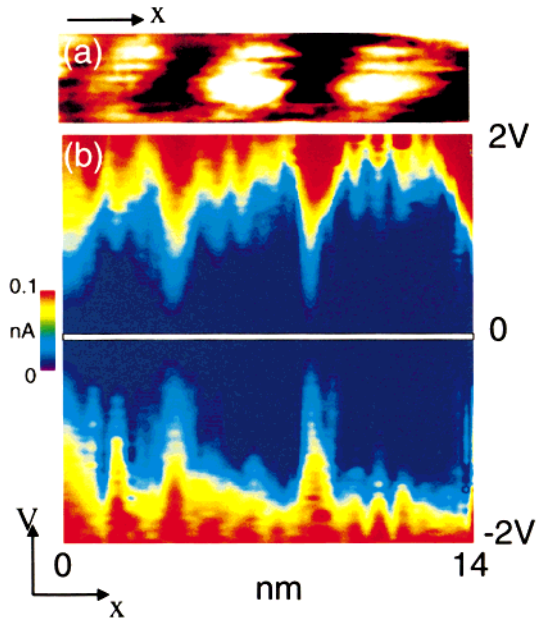

Figure 6. (a) STM image of three Ag nanoparticles from the same insulating monolayer shown in Figure 5 and (b) corresponding *I*−*V* map. The *x*-axis in (b) is the topographic direction and the *y*-axis is the bias voltage. The *z*-axis (represented by the color scale) corresponds to the tunneling current at a given x-position and bias voltage, averaged over the vertical column in (a) with the same *x* values. Little or no tunneling current at the particles is consistent with previous figures. The width of the dark region (the Coulomb blockade) at each position indicates the Coulomb gaps of the different particles as presented in Figure 5. (see text for details)

The effect of disorder has been also studied theoretically by Remacle and Levine. They have recently reported on a full quantum mechanical model of NC superlattices, and they explicitly addressed the role of disorder.[16] They found three distinct regimes, depending on the interparticle separation distance. At large separation, the superlattice is a Mott insulator, with a Coulomb gap that is related to the single particle charging energy of the individual NCs. As the monolayer is compressed, this gap closes (the Mott insulator−metal transition), but the superlattice is still in the insulating state because of disorder-induced localization (so-called Anderson localization). The localized insulator exists only over a very narrow range of $D/2r$ values, and Remacle and Levine predict that it should be easier to observe in larger particles. Upon further compression the superlattice becomes truly metallic. On the basis of their theoretical prediction and our experimental results, the disorder of a monolayer produces localized state and electron conduction happens through variable range hopping.

4.2. Wide Coulomb Gaps. In the insulating monolayers of Ag NCs, we have not only confirmed the insulating nature of the particle films with large $D/2r$, but also have discovered two distinct types of insulating monolayers. The square lattice film exhibits two electronically distinct lattice sites, while the hexagonal lattice structure film contains electronically homogeneous NCs. Half of the NCs in the square lattice film show unusually wide Coulomb gaps, which is opposite to what we expect as we construct a network of capacitively coupled NCs. In order to understand the origin of this unusual gap, we first summarize what we have observed in the two insulating films.

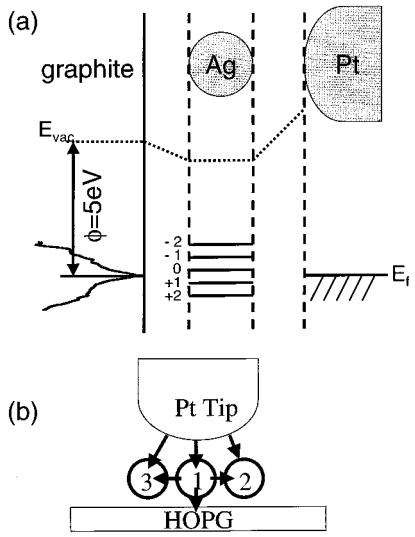

Figure 7. (a) Energy level diagram for the tip−particle layer−substrate system at zero bias. The dotted line represent the vacuum level. For the graphite substrate, the NDOS is plotted from the experimental results showing semimetal behavior. (b) Dynamic tunneling as the tip bias is applied. The tip, central particle, neighboring particles, and substrate for a complex system must be considered as a whole.

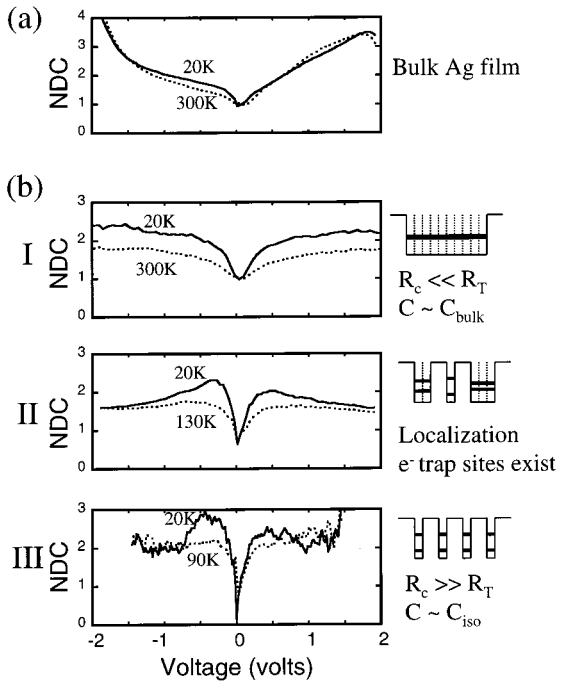

Figure 8. Temperature dependence of the NDC of (a) a bulk Ag film and (b) three different Ag nanocrystal monolayer films. The spectra in (a) were collected from a Ag film thermally evaporated onto a HOPG surface. In (b), three different types of NDC are shown from metallic (I), intermediate (II), and insulating (III) films. On the right-hand sides of each plot, simple sketches for particle coupling schemes are illustrated. (R_c = contact resistance between particles; R_T = quantum contact resistance (~13 kΩ).)

Only the moderately disordered square lattice film contains wide-gap particles, and next to these, there are always some nearest-neighbor normal gap particles. In Figure 7a, we also examine the electronic structure of our system. Although the absolute positions of the Coulomb charging states of Ag NCs cannot be determined precisely, the Fermi level should be located between two charging states, 0 and +1 states for example. Various fluctuations, such as the radius, in the particle may cause the residual static charges on the NCs to vary from particle to particle. In addition, graphite is a semimetal that is poorly coupled electronically to the particle film, which restrains vertical current flow.

On the basis of the observations and the energy level diagram, we examine the effects of the neighboring particles, substrate, and tip shape. Since tunneling to the HOPG is a slow process, tunneling to neighboring particles is an important channel. Therefore, the secondary current path can play a significant role. The tip is large compared to the particle size, and thus the neighboring particles are placed under a bias voltage. Finally, the neighboring particles are not only coupled capacitively to the center particle being scanned, but charge on them can gate the current flow on the central particle. This issue has been studied theoretically[17] and also observed previously.[8] From these effects, the neighboring particles gate the center particle and at the same time they change their charging states according to the electric potential applied to the tip. This may result in the wide range of the gating region and cause the increase in the Coulomb gap. However, this explanation is by no means certain, and we are now pursuing a series of experiments to systematically examine the various influences on the tunneling to a NC in an array.

4.3. MI Transition. Figure 8 summarizes the electron transport behavior of monolayer Ag NC films as determined in this study. As we construct superlattices of Ag particles, three parameters, D, $2r$, and ordering, play important roles. Depending on these parameters, three types of NDC are plotted in (b). For small $D/2r$ (case I, metallic film), the contact resistance is close to zero and electrons are delocalized. NDC is unity at zero bias and the overall shape resembles the bulk Ag film shown in (a). In case II, the hopping-conduction film, NDC is neither unity nor zero. Also, we have observed the temperature dependence of the conductance spectra. Disorder in the monolayer creates localization regimes, and this is believed to be responsible for the temperature dependence as pointed by Remacle and Levine.[16] The VRH model is proposed to explain this behavior. For large $D/2r$ (case III, insulating film), the contact resistance between the particles is too big for electrons to move freely over the film. The Coulomb gap is clearly shown in the NDC plot and at zero bias the NDC is zero.

We observe three different conductivity regimes, where for ordered monolayers the ratio of two parameters, D and $2r$, determines whether the film is metallic or insulating, as previously observed using ac spectroscopy.[5−7] We demonstrate here, using dc spectroscopy, the validity of the previous results. Under the dc transport point of view, we also arrive at the same situation demonstrated by Collier[5] and Shiang,[6] where classical coupling between particles is not sufficient to explain the MI transition. Note that the capacitance of each particle is affected by its nearest neighbors (and substrate), reducing the Coulomb charging energy. Therefore, for the monolayer film of 4.8 nm particles, we have a quantum mechanical coupling that delocalizes the electron wave functions.

5. Conclusions

We studied the electronic properties of isolated particles and of superlattices assembled from silver NCs of different sizes. Many results were consistent with our previous work on isolated and exchange-coupled NC superlattices,[8] but significant new physics was also observed. All isolated particles supported by metallic substrates exhibited a Coulomb gap, regardless of particle size or passivating ligand. For two-dimensional superlattices of NCs, we observed four unique types of behavior. Monolayer superlattices of 4.8 nm octanethiol-passivated NCs

($D/2r \sim 1.25$) exhibited true metallic behavior, including no Coulomb gap and a temperature-independent finite-valued DOS at 0 V. Monolayer superlattices of 6.6 nm dodecanethiol-capped Ag NCs ($D/2r \sim 1.3$) exhibited relatively featureless current−voltage curves and no evidence of a Coulomb gap. However, the conductivity of these films near 0 V exhibited a temperature dependence consistent with variable range hopping in a two-dimensional lattice, and these films are possibly the localization-induced insulators predicted by Remacle and Levine to occur at $D/2r$ values intermediate between a Mott insulator and a true metallic film. We observed normal insulating films consisting of 2.7 nm diameter Ag cores passivated by hexanethiol ligand. The lattice was hexagonal and well-ordered and exhibited the expected Coulomb gap. For square superlattices consisting of 2.7 nm diameter Ag cores and a $D/2r$ value of $\sim$1.4, we observed strong insulating behavior in the film, and two distinct types of superlattice sites. Half of the superlattice sites were characterized by charging energies that were in the range expected for isolated particles, but the other half were characterized by anomalously large charging energies. We believe that this latter effect may be caused by a dynamic gating effect.

Acknowledgment. The authors thank Dr. J. F. Sampaio and Prof. F. Remacle for many helpful discussions. J.R.H. and S.-H.K. were supported in part by an NSF-GOALI grant, the David and Lucille Packard Foundation, and a Sloan Fellowship.

References and Notes

(1) Springholz, G.; Holy, M.; Pinczolits, M.; Bauer, G. *Science* **1998**, *282*, 734.

(2) Medeiros-Ribeiro, G.; Bratkovski, A. M.; Kamins, T. I.; Ohlberg, D. A. A.; Williams, R. S. *Science* **1998**, *279*, 353.

(3) Murray, C. B.; Kagan, C. R.; Bawendi, M. G. *Science* **1995**, *270*, 1335.

(4) Collier, C. P.; Vossmeyer, T.; Heath, J. R. *Annu. Rev. Phys. Chem.* **1998**, *49*, 371.

(5) Collier, C. P.; Henrichs, S. E.; Shiang, J. J.; Saykally, R. J.; Heath, J. R. *Science* **1997**, *277*, 1978.

(6) Shiang, J. J.; Heath, J. R.; Collier, C. P.; Saykally, R. J. *J. Phys. Chem. B* **1998**, *102*, 3425.

(7) Markovich, G.; Collier, C. P.; Henrichs, S. E.; Remacle, F.; Levine, R. D.; Heath, J. R. *Acc. Chem. Res*. **1999**, *32*, 415.

(8) Medeiros-Ribeiro, G.; Ohlberg, D. A. A.; Williams, R. S.; Heath, J. R. *Phys. Rev. B* (brief reports) **1999**, *59*, 1633.

(9) Heath, J. R.; Leff, D. V.; Knobler, C. M. *J. Phys. Chem*. **1997**, *101*, 189.

(10) Korgel, B. A.; Fitzmaurice, D. *Adv. Mater*. **1998** *10*, 661.

(11) Sear, R. P.; Chung, S.-W.; Markovich, G.; Gelbart, W. M.; Heath, J. R. *Phys. Rev. E*, in press.

(12) Dorogi, M.; Gomez, J.; Osifchin, R.; Andres, R. P.; Reifenberger, R. *Phys. Rev. B* **1995**, *52*, 9071; Andres, R. P.; Bein, T.; Dorogi, M.; Feng, S.; Henderson, J. I.; Kubiak, C. P.; Mahoney, W.; Osifchin, R. G.; Reifenberger, R. *Science* **1996**, *272*, 1323.

(13) Wiesendanger, R. *Scanning Probe Microscopy and Spectroscopy: Methods and Applications*; Cambridge University Press: Cambridge, UK, 1994; p 139.

(14) Mott, N. F.; Davis, E. A. *Electronic Processes in Noncrystallince Materials*; Clarendon Press: Oxford, UK, 1971.

(15) For more discussion on the VRH model, see for example: Shklovskii, B. I.; Efros, A. L. *Electronic Properties of Doped Semiconductors*; Springer-Verlag: Berlin, 1984; Chapter 9.

(16) Remacle, F.; Levine, R. D. To be published.

(17) Hanna, A. E.; Tinkham, M. *Phys. Rev. B* **1991**, *44*, 5919.